Journal of Drug Delivery Science and Technology 108 (2025) 106901

Contents lists available at ScienceDirect

Journal of Drug Delivery Science and Technology

journal homepage: www.elsevier.com/locate/jddst

Evaporation-triggered nanoprecipitation for PLGA nanoparticle formation using a spinning-disc system

Alexandra J. Zander [a], Marie-Sophie Ehrlich [a], Saad ur Rehman [a,b], Marc Schneider [a,b,*]

[a] Department of Pharmacy, Biopharmaceutics and Pharmaceutical Technology, Saarland University, Campus C4 1, D-66123, Saarbrücken, Germany
[b] PharmaScienceHub (PSH), Campus A2 3, D-66123, Saarbrücken, Germany

ARTICLE INFO

Keywords:
Polymeric nanoparticles
Nanotechnology
Drug loading
Size tuning
Up scaling

ABSTRACT

Researchers have successfully introduced many formulations based on nanoparticles and many of those products are already available for clinical use. When it comes to polymeric nanoparticles, there are only natural polymers (*e.g.*, albumin) approved but several publications describe very promising results at the laboratory level. Poly (lactic-*co*-glycolic acid) (PLGA) is widely used by researchers to prepare nanoparticles and there are several publications available with very promising results at the laboratory level but there are barely any approaches for commercial production of PLGA nanoparticles. One of the main challenges is the difficulty in converting lab scale production into commercial scale production. This study describes a very innovative manufacturing technology *i.e.* spinning disc system (SDS) for the continuous manufacturing of PLGA nanoparticles. It relies on a one-pot process, *i.e.* polymer, organic phase, aqueous phase and drug are homogeneously distributed and mixing as critical process parameter is eliminated. Centrifugal force causes the solution to spread all over the rotating disc and the large surface area of the disc facilitates the evaporation of the organic phase resulting in polymer precipitation. This manufacturing method also enables tuning of particle size (a wide range of between 120 and 320 nm can be achieved). Compared to standard bench top (BT) methods, smaller particles with higher yields were obtained (141 nm with a yield of 89 %). Along with continuous production of nanoparticles, SDS also improves encapsulation efficiency and drug loading of PLGA nanoparticles. Curcumin (CUR) as a model drug substance was encapsulated with SDS with a high encapsulation efficiency (60–70 %) compared to only 10–25 % in BT. Subsequently, a drug loading twice as high as with BT was achieved using SDS. The nanoparticles prepared with or without stabilizer produced nearly monodisperse particle sizes (PDI <0.1) and showed negative zeta-potentials (<−30 mV), which showed promising colloidal stability over a test period of 28 days. Maximum 7.4 nm of deviation from initial size was observed in stability studies.

Abbreviations

SDS	Spinning disc system
BT	Bench top
PLGA	Poly (lactic-*co*-glycolic acid)
LA	Lactic acid
GA	Glycolic acid
CUR	Curcumin
PVA	Polyvinyl alcohol
ACE	Acetone
ACN	Acetonitrile
THF	Tetrahydrofuran
DL	Drug loading
EE	Encapsulation efficiency
PDI	Polydispersity index
RC	Regenerated cellulose
SEM	Scanning electron microscopy

1. Introduction

Within the last three decades, a considerable amount of research has been devoted to polymeric biomaterials, with poly (lactic-*co*-glycolic acid) (PLGA) being the most extensively studied. PLGA is a biocompatible, biodegradable polymer that has been approved for medical use by the FDA for decades. A selection of approximately 20 depot formulations such as the microparticulate Lupron Depot®, the solid implant

* Corresponding author. Biopharmaceutics and Pharmaceutical Technology, Saarland University, Campus C4 1, D-66123, Saarbrücken, Germany.
E-mail address: Marc.Schneider@uni-saarland.de (M. Schneider).

https://doi.org/10.1016/j.jddst.2025.106901
Received 21 August 2024; Received in revised form 27 March 2025; Accepted 5 April 2025
Available online 11 April 2025

Propel® and the *in situ* gel Perseris™ are available [1]. PLGA is also the most widely used polymer for nanoparticulate drug delivery vehicles and a large variety of small molecules [2] and macromolecules such as peptides [3,4], proteins [5,6] and DNA/RNA [7] were successfully formulated. Nanoparticulate formulations can increase solubility and improve bioavailability of poorly soluble drugs by increasing the surface area, as well as enable modified release of drugs by degradation of the polymer and modification of the particle surface.

However, so far there are no therapeutics on the market that use PLGA in nanoparticulate formulations. This might be due to the fact that no cost- and time-efficient mass production process for pharmaceutical manufacturers has existed so far, which limits the potential clinical application. Currently, there are a few approaches for large-scale production of PLGA nanoparticles, *e.g.* the semi-automated nanoprecipitation-system developed by Rietscher and colleagues [8], the nanoprecipitation system based on MicroJet Reactor (MJR) technology [9] or the emulsion solvent-evaporation technique modified by Schiller et al. [10] using focused ultrasound or in general microfluidic approaches [11,12]. As particles must be subsequently purified from solvents or stabilizers before use, this represents a further time and cost consuming factor for commercial production.

A spinning disc is a multifunctional device promising automated mass production at reasonable costs for the manufacturer. These systems provide a continuous flow process in which high centrifugal forces are used to disperse the liquid impinging on the rotating disc into a thin film, thus creating a large surface to volume ratio of the liquid. This technology has been used for decades *e.g.,* to carry out various fast chemical reactions in so-called spinning disc reactors (SDR), including reactions of polymerization [13], neutralization [14] and re-crystallization [15]. In addition, a large number of nanosized chemical compounds were produced via reactive precipitations *e.g.,* hydroxyapatite [16], TiO_2 [17], ZnO [18] as well as magnetic Fe_3O_4 [19,20]. As described in literature, spinning disc technology has successfully been used for ionic gelation of chitosan nanoparticles [21] and for solvent-antisolvent precipitation of nanoparticles consisting of *beta*-carotene [22], starch [23] or curcumin [24]. What they have in common is a two-phase feeding of the reacting liquids, thus taking advantage of the fast and homogenous micromixing capability of the rotating disc [16,25]. In addition, this technology enables an increased and controllable heat and mass transfer, which supports many syntheses and processes that are otherwise limited in this respect [26]. This also applies to concentrate liquids, as described by Akhtar et al. [27], representing a gentle method due to short contact time to a heated plate.

Besides methods like emulsion solvent-evaporation, salting-out and electrospray drying, solvent-antisolvent precipitation is a commonly used technique for preparation of PLGA nanoparticles [28–30]. The precipitation mechanism is described in literature as a four-step process: supersaturation, nucleation and growth by condensation and coagulation. The addition of dissolved polymer to the antisolvent, in which the solvent is fully miscible, results in reduced solubility and leads to supersaturation when the equilibrium saturation concentration is exceeded. Above the critical supersaturation concentration nucleation is induced [31,32]. Solvent-antisolvent precipitation is often used in the classical bench top (BT) production process. Here, the polymer dissolved in a solvent is added from a syringe through a small needle under stirring into the container filled with the antisolvent. Thus, due to the miscibility of the solvent and the antisolvent solubility of the polymer is reduced and the critical supersaturation is reached by diffusion. For our modified precipitation method, a well-mixed water fraction in an organic phase with a vapor pressure higher than water is used. Subsequently, evaporation of the organic phase will reduce polymer solubility achieving supersaturation. This process is accelerated by dropping the polymer-containing mixture on a rotating disc. The thin film formed by the centrifugal forces increases the interface for solvent evaporation, reaching faster the critical supersaturation. When the equilibrium saturation concentration of the polymer is exceeded, supersaturation is achieved and above to the critical supersaturation concentration particle nucleation is induced (Sketch 1). As a result, a nanoparticle suspension in the antisolvent is obtained.

Aim of the current work was to manufacture PLGA nanoparticles of uniform and tunable size in an experimental SDS by evaporation-controlled nanoprecipitation. To understand effects on particle formation parameters such as the solvents-antisolvents used, the block-copolymer ratios and polymer concentration was varied as well as operational parameters (spinning speed and dripping position) were tested. Resulting NPs were characterized with respect to size, zeta potential, yield, and surface morphology. The stability of stabilizer-containing and stabilizer-free nanoparticles was also investigated. Drug loading and encapsulation efficiency were evaluated using curcumin (CUR) as hydrophobic, fluorescent model substance in comparison to the BT approach. Transferability of nanoparticle preparation to a modified prototype allowing in principle for continuous production was tested.

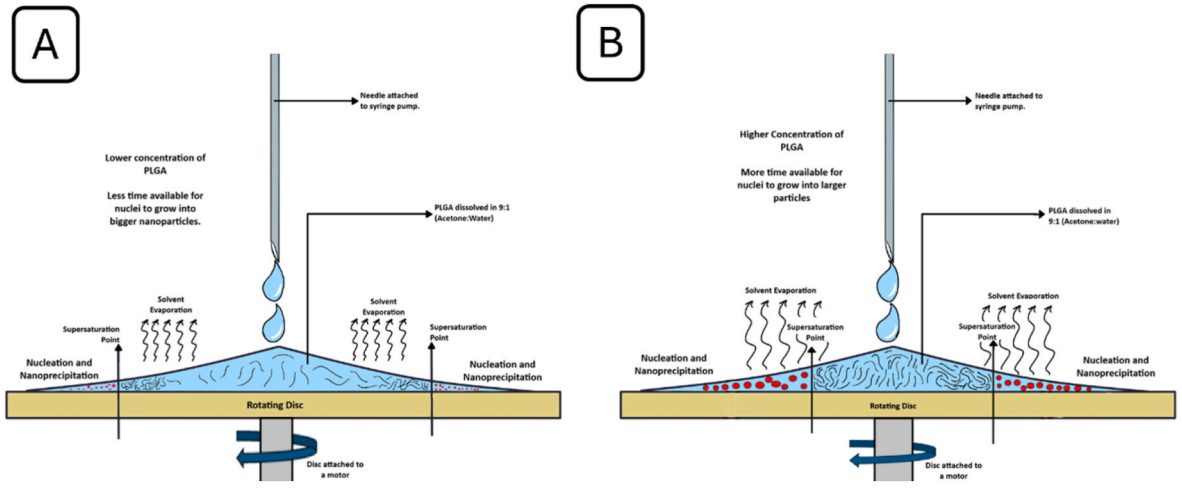

Sketch 1. (A) Illustration of the lateral view of the spinning/rotating disc with higher concentration of PLGA and (B) lower concentration of PLGA in solvent-antisolvent mixture. Considering the same rotation speed and flow rate, supersaturation point might be achieved earlier in the case of higher concentration and therefore the formed nuclei will have more time (due to larger distance to edge of disc) and more polymer available to grow into bigger nanoparticles. Whereas in the case of lower concentration, supersaturation point might be achieved later as compared to higher concentration and therefore, the formed nuclei will have less time and less polymer available to grow into bigger nanoparticles.

2. Materials and methods

2.1. Materials

PLGA [50:50 lactic acid:glycolic acid (LA:GA) with M_W 7000–17,000 g/mol (Resomer RG502H), M_W 24,000–38,000 g/mol (Resomer RG503H) and M_W 38,000–54,000 g/mol (Resomer RG504H); 65:35 LA:GA of M_W 24,000–38,000 g/mol (Resomer RG653H); 75:25 LA:GA of M_w 22,000–36,000 g/mol (Resomer RG753H)] were purchased from Evonik Industries AG (Essen, Germany). CUR was obtained from Sigma Aldrich (Steinheim, Germany). Polyvinyl alcohol [PVA, M_W ~31,000 (Mowiol® 4–88)] was provided by Kuraray Europe (Hattersheim, Germany). Acetone (ACE, analytical reagent grade), acetonitrile (ACN, HPLC gradient grade), tetrahydrofuran (THF, analytical grade) and ethanol (HPLC grade) were purchased from Fisher Scientific Ltd (Loughborough, UK). Methanol and isopropanol, both HPLC grade, were purchased from VWR International (Darmstadt, Germany). Water used was Millipore Q-Gard 2 by water purification system from Merck Millipore (Billerica, USA). Sulfuric acid was purchased from Bernd Kraft GmbH (Duisburg, Germany).

2.2. Experimental setup - spinning disc systems

2.2.1. Prototype I

The developed simple prototype I is composed of several modules (Fig. 1A, left scheme). A modified, propeller less computer fan (12 × 12 cm, AVC, Taipei, Taiwan) represents the core of the system. The lid of a glass petri dish (Steriplan 15 × 100 mm, Brand GmbH Co KG, Wertheim, Germany) is permanently fixed upside down on the engine of the fan as holder for the petri dish base, which is inserted into the lid and fixed using a rubber band. It serves as an exchangeable precipitation and collection vessel. A laboratory power supply unit (EA-PS 2323A, EA Elektro-Automatik GmbH & Co.KG, Viersen, Germany) supplies power to the fan with variable voltage to adjust the rotation speed of fan and petri dish. The rotational speed of the inserted petri dish was determined with a tachometer (Voltcraft® DT-10L, Conrad Electronic AG, Wollerau, Switzerland). A syringe pump (PHD 2000 programmable, Harvard Apparatus Inc., Holliston, USA) was used to adjust the flow rate of the polymeric solvent-antisolvent mixture to the inserted, rotating petri dish. The tip of the needle (0.55 × 25 mm) fixed on a syringe (5 ml–20 ml), all purchased from B. Braun Melsungen AG (Melsungen, Germany), was positioned approx. 3 mm above the inserted petri dish.

2.2.2. Prototype II

For continuous sample collection, a second prototype was constructed using a special glass vessel. It included a round recess for the engine of the fan with indentations as protection against leakage and a sample release at the bottom (Fig. 1A, right scheme). The polymeric solvent-antisolvent mixture was dripped on a glass petri dish lid, which was fixed in proper alignment on the engine of the fan. With the new prototype larger quantities of liquid could be applied and, thus, nanoparticle production for increased quantities was possible.

2.3. Particle preparation

2.3.1. Nanoprecipitation by evaporation-triggered SDS

For preparations of polymeric nanoparticles, 10 mg Resomer RG 503H was dissolved in 4.5 ml ACE while stirring rigorously for 10 min before 0.5 ml water was added. Due to the volume contraction when mixing water and acetone, the obtained volume is reduced, and thus, the polymeric concentration is increased. However, this effect is low (4.5 ml water + 0.5 ml of acetone yields a volume reduction of 50 µl) and therefore, this effect is neglected and the originally used volumes are utilized. As standard preparation, 2 % (w/v) PVA solution was used to coat the inserted rotating disc by drying at ambient conditions. Afterwards the polymeric solvent-antisolvent mixture was applied to the disc. The pre-coated disc allowed the water-soluble PVA to dissolve and to stabilize the precipitated and freshly formed nanoparticles. The engine of the fan was started at 5 V corresponding to a measured rotational speed of approximately 841 rpm. The solution was applied to the center of the rotating plate at a syringe pump flow rate of 0.5 ml/min. The resulting nanoparticle dispersion was removed from the rim of the inserted petri dish (prototype I). The designated parameters were used in the following investigations (standard procedure) unless otherwise stated.

2.3.2. Influence of different parameters on NP size

To investigate the influence of system specific settings on particle size, spinning speeds of 841 rpm (5 V), 2051 rpm (5.5 V) and 2727 rpm (7 V) and positions of the needle for solution application of 0, 1.5 and 3 cm distance from the center of the inserted petri dish were tested.

The dependence of polymer type, polymer concentration, and solvent composition on nanoparticle size was also investigated. For polymer types, different molecular weights of 50:50 LA:GA ratio (Resomer RG 502H, 503H, 504H), different LA:GA ratios (Resomer RG 503H, 653H, 753H) and PLGA concentrations of 0.5–22 mg/ml of Resomer RG

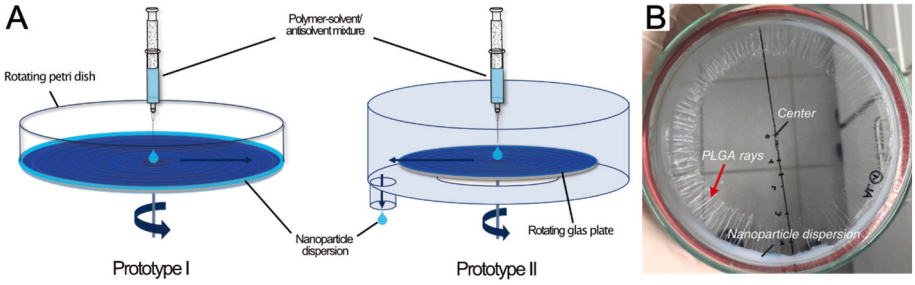

Fig. 1. Nanoprecipitation by solvent-evaporation in a spinning disc system. A: Schematic illustration of spinning disc setups. Blue arrows display movements of the plates and the fluid. B: Petri dish after nanoprecipitation with centered dropping position. At a certain distance from the center of the plate, radially arranged dried polymer residues can be found (red arrow). Nanoparticle dispersion accumulates in the rim of the dish. (For interpretation of the references to colour in this figure legend, the reader is referred to the Web version of this article.)

503H were used.

The influence of solvent and antisolvent on particle size was investigated comparing ACE, ACN, and THF as solvents and water, ethanol, methanol, and isopropanol as antisolvents. To demonstrate the evaporation effect on particle formation solvent-antisolvent mixtures were prepared as described above but dried on non-rotating silica wafers depositing precipitated nanoparticles which could then be used for SEM imaging.

2.3.3. Nanoprecipitation by standard BT process

Different concentrations of Resomer RG 503H as well as different types of PLGA were compared regarding sizes of resulting nanoparticles prepared by commonly used nanoprecipitation. In brief, Resomer RG 503H in masses of 10–40 mg and different PLGA types (Resomer 502H, 503H, 504H, 653H and 753H) at a mass of 25 mg were dissolved in 1.5 ml ACE for 10 min under rigorous stirring. Polymeric solutions were then added to 10 ml of aqueous solution containing 2 % (w/v) PVA under stirring using a syringe pump adjusted to an injection rate of 0.5 ml/min. The resulting nanoparticle dispersion was purified by centrifugation at 10,000×*g* for 20 min and redispersed in fresh MilliQ water. This washing procedure was repeated twice to remove solvent and excess stabilizer. It is noteworthy that the SDS product consisted of a small volume in total consisting of presumably mainly antisolvent phase at high particle concentration in contrast to the BT product having a higher sample volume in total consisting of a larger antisolvent volume and a minor solvent volume and containing a low particle concentration before purification.

2.3.4. CUR-loading of NPs

For preparation of CUR-loaded nanoparticles, CUR was dissolvent in ACE to yield a 1 % (w/v) solution. In SDS (prototype I), Resomer RG 503H was dissolved in ACE and CUR solution was added to obtain polymer concentrations of 2, 6 and 12 mg/ml and an initial drug content of 1 % (w/w) to the polymer. In another experiment, a polymer concentration of 6 mg/ml and initial drug contents of 1, 2 and 5 % (w/w) with respect to the polymer were prepared. The resulting nanoparticle dispersion was collected and centrifuged at 10,000×*g* for 20 min (Rotina 420R, Andreas Hettich GmbH & Co.KG, Tuttlingen, Germany). The supernatant was discarded to eliminate free non-encapsulated drug.

In BT, CUR-loaded nanoparticles were prepared with an initial polymer concentration of 12 mg/ml and purified in the same way as described in section 2.3.3. Nanoprecipitation by standard BT process, ACE was partially replaced by CUR stock solution (1 % (w/v) in ACE) to obtain initial concentrations of 1, 2 and 5 % (w/w) of the polymer. Qualification (DL and EE) were processed as described in section 2.5.3. CUR quantification.

2.3.5. Transferability to prototype II

Testing the transferability to prototype II, polymeric solvent-antisolvent mixture was prepared in an amount of 20 ml and precipitated under same system parameters as used for prototype I. The spinning disc was not coated with PVA, as the amounts of coating material used in prototype I, is not sufficient for larger amounts of polymer used in prototype II (2.3.1. Nanoprecipitation by evaporation-triggered SDS). The collection vessel was pre-wetted with water to increase the liquid volume and allow the produced nanoparticles dispersion to be collected without sticking to the walls.

2.4. Determination of yield and evaluation of NP stability

The yield was determined by freeze-drying freshly manufactured and collected nanoparticle dispersions, prepared from starting concentrations of 2, 6 and 12 mg/ml (alpha 3–4 LSCbasic, Martin Christ Gefriertrocknungsanlagen GmbH, Osterode am Harz, Germany). The freeze-drying process was running over 24 h.

The colloidal stability of nanoparticles (Resomer RG 503H in prototype I) prepared with and without PVA coating of the disc was investigated in prototype I. Therefore, the resulting dispersion was stored at 4 °C and the quality with respect to the colloidal properties (size, PDI and ζ-potential) was evaluated on freshly prepared particles and after 7, 14, 21 and 28 days by dynamic light scattering measurements. For prototype II, the stability was only investigated for PVA-free conditions.

2.5. Particle characterization

2.5.1. Particle size, polydispersity index and ζ-potential

Nanoparticle size and polydispersity index (PDI) were determined using dynamic light scattering, ζ-potential was measured by using electrophoretic light scattering (Nano ZS, Malvern Panalytical GmbH, Malvern, UK and Almelo, the Netherlands). The analysis was performed at a backscatter angle of 173° and at 25 °C using samples appropriately diluted with MilliQ-water and filled in folded capillary zeta cells (DTS1070, Malvern Panalytical, Malvern, UK and Almelo, the Netherlands).

In the case of samples precipitated directly on silica wafers, for the evaluation of the evaporation effect on particle formation from different solvent-antisolvent mixtures, particle sizes were investigated using SEM imaging. For size evaluation, 30 randomly chosen particles were measured by Fiji (version 1.0).

2.5.2. Particle morphology

The surface morphology of dried samples was determined by scanning electron microscopy (Zeiss EVO 15, Carl Zeiss AG, Oberkochen, Germany). Samples were diluted with MilliQ-water, dropped on a silica wafer and dried under ambient conditions. After sputtering with a 10 nm gold layer under vacuum conditions (Q150R Rotary-Pumped Sputter Coater, Quorum Technologies Ltd., Lewes, UK) the samples were imaged at a working distance of 16.5 mm and an acceleration voltage of 5 kV. When evaluating the evaporation effect on particle formation from different solvent-antisolvent mixtures, the particles were precipitated directly on the wafer and then treated as described above for imaging.

2.5.3. CUR quantification

Samples for quantification of CUR were freeze-dried for 24 h and quantified regarding drug loading (DL) and encapsulation efficiency (EE). Therefore, the particles were dissolved in ACN (1 mg/ml), filtered (0.45 μm, RC membrane filter Titan 3, Thermo Fisher Scientific Inc., Waltham, USA) and analyzed by fluorescence spectroscopy (plate reader Infinite M200, Tecan Trading AG, Männedorf, Switzerland). The excitation and emission wavelengths were set to 415 nm and 515 nm respectively. The calibration curve used for calculation of CUR concentration was linear in the range of 0.1–1 μg/ml. Drug loading content in percent of the formulation weight (DL%) and encapsulation efficiency in percent of originally used amount (EE%) were calculated using equations (1) and (2).

$$DL[\%] = \frac{w_{drug\ in\ 1\ mg\ formulation}}{1\ mg} \times 100\% \quad (1)$$

$$EE[\%] = \frac{w_{recovered\ drug}}{w_{initial\ drug}} \times 100\% \quad (2)$$

2.6. Determination of residual solvent in samples prepared by SDS

Residual acetone was determined by using HPLC analysis. 3 mM sulfuric acid and 100 % ACN were used as mobile phase. A flow rate of 0.8 ml/min on a reverse-phase column (LiChrospher® 100 RP-18 5 μm) was used for the analysis. Sample for HPLC analysis was prepared by taking 100 μl of NPs suspension after preparation from the respective collection volume. Samples were analyzed for different rotation speeds as well as for different time points after preparation for a SDS setup with

1000 rpm. The suspensions were dissolved in 5.0 ml of ACN. 20 µl from these samples was then analyzed using HPLC at λ = 260 nm. Standards of acetone were also prepared for generating the respective calibration curve (Fig. S2).

3. Results and discussion

3.1. Nanoprecipitation by evaporation-triggered SDS

We were able to produce particles using SDS based on a modified nanoprecipitation technique. The large surface of the rotating plate triggered extensive evaporation of the applied solvent (ACE). Thus, nanoparticles precipitated and produced a milky, highly concentrated nanoparticle dispersion in the small amount of antisolvent (Fig. S1). However, a loss of polymer on the rotating plate was visible (Fig. 1B), being thoroughly described in section 3.3. An assumed preparation volume of 5 ml, simplified regarding the previously mentioned volume contraction effect adding water to acetone, resulted in a dispersion volume of 0.3–0.4 ml. Depending on the parameters for preparation the solvent component (4.5 ml) was completely removed by evaporation which was shown by HPLC (Fig. 7). Therefore, it is obvious that water evaporation has also occurred during particle production.

3.2. Influence of different parameters on NP size

3.2.1. Effect of PLGA concentration

Higher PLGA concentrations resulted in larger particles for SDS and BT method (Fig. 2). In the latter case, however, the effect was less pronounced. The dependence of particle size on polymer concentration for BT was already described by Huang and Zhang [33].

Within the concentration range tested, sizes of approx. 120–380 nm were achieved using the SDS (Fig. 2A). Up to a concentration of 16 mg/ml, an almost linear relationship between polymer concentration and particle size could be observed. Above a concentration of 16 mg/ml, fluctuating sizes of 335–380 nm display limited reproducibility, indicating that a plateau was reached, or a maximum controllable particle size was exceeded. The particle size distribution became wider with increasing polymer concentration, which is indicated by an increasing PDI from 0.016 to 0.2 correlating with the particle size. However, in the linear range, the PDI did not exceed 0.2 indicating still a narrow distribution [34]. Using the BT method, particle sizes of approx. 150–220 nm with very narrow size distributions (PDI <0.1) were achieved (Fig. 2B). When using higher concentrations of 50 mg and more dissolved in 1.5 ml ACE to produce larger nanoparticles, no homogeneous nanodispersion was achieved, and visible precipitates formed directly at the tip of the cannula. Bilati et al. [35] also reported unsuccessful nanoprecipitation at higher concentrations in the BT system. Huang and Zhang [33] did not report any further increase in size at a higher concentration than 20 mg/ml, but only an increase in particle size distribution by measuring individual, larger particles. We suspect that at higher polymer concentrations supersaturation is faster achieved, and thus, an earlier precipitation of the polymer is the result (sketch 1 A and B). In the classical BT system, higher concentrations lead to shorter diffusion distances of the polymer molecules to reach the next. This increases the probability of collision and larger particle formation. For SDS, diffusion should not affect the solution as it is already premixed. Due to reaching the solubility limit, process of nucleation triggers and particles grow, which will lead to increasing particles with increasing polymer concentration. The precipitation process with higher polymer concentrations starts at a lower distance from the center of the spinning disc due to the faster reached supersaturation. Anantachoke et al. assumed that the distance between the polymer chains thereby is lower and therefore their collision probability is higher [22]. The higher number of polymer chains per volume, which is associated with the increase in concentration, increases the probability of particles growth which is observed. It appears that reduced diffusion in the BT system has a less pronounced effect on the particle size than the distance effects in SDS as a consequence of the centrifugal forces and solvent evaporation.

3.2.2. Effect of PLGA types

As shown in Fig. 3A and B, PLGA types did not influence the investigated particle size during nanoparticle production using the BT method. Particle sizes were constant around 180–195 nm and uniform, low PDIs of <0.1 were achieved. Budhian et al. also reported unchanged particle sizes at different inherent viscosities and LA contents in BT method [36]. In contrast, the evaporation-triggered method using SDS led to significantly larger particles with increasing LA content in the polymer (Fig. 3A), approximately 140 nm for LA:GA 50:50 compared to 230 nm for LA:GA 75:25. A higher proportion of LA in the polymer implies increased hydrophobic interactions and lower number of possible hydrogen bonds. This leads to a lower solubility of the polymer in the aqueous medium and thus the polymer phase reaches faster supersaturation. Due to this effect happening earlier, the nucleation happens at a higher density of nuclei. Consequently, the nucleation process leads to particle increase due to a higher probability of collision or the adsorption of free polymer [37]. This effect is probably less pronounced for the setting of the BT method as no differences in particle size could be measured. However, Bilati et al. [35] described that in case of using other parameters such as a different solvent, the LA:GA ratio might also affect particle sizes in BT method.

With increasing viscosity or increasing molecular weight, smaller particles were obtained in SDS (Fig. 3B). The lowest molecular weight (7000–17,000 g/mol) produced particles almost twice as large as the highest molecular weight (38,000–54,000 g/mol) (243.3 ± 5.7 nm vs.

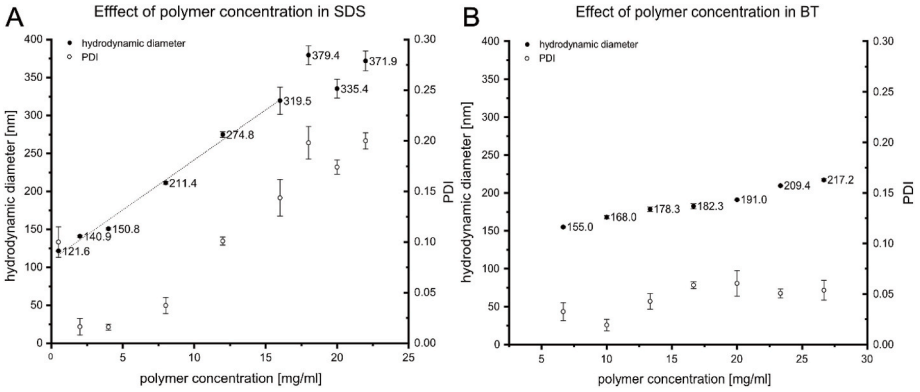

Fig. 2. Effect of polymer concentration on nanoparticle size. A: DLS results for PLGA NP formation in dependence of the used concentration using SDS. Trend line ($R^2 = 0.99216$) indicates a nearly linear relationship between polymer concentration up to 18 mg/mL and particle size. B: DLS results for NP sizes using different PLGA concentrations in the BT setup.

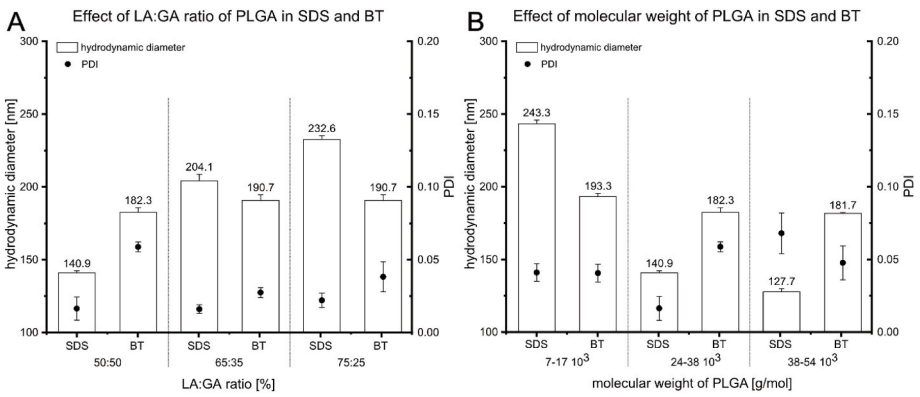

Fig. 3. Effect of polymer types on sizes of nanoparticles precipitated by SDS and BT. A: Different LA contents of PLGA. B: Different molecular weights of PLGA.

127.7 ± 2.2 nm), whereas the difference in size between the medium molecular weight PLGA (24,000–38,000 g/mol) and the highest molecular weight PLGA (10–15 nm) was rather small. This may be explained by the overlap of the molecular weights of both polymers.

Crucho and Barros [38] reported opposite behavior in the BT method. According to their data, higher viscosity should make diffusion of the two solvents into each other slower and thus produce larger particles. This argument of solvent diffusion does not apply to the prefabricated solvent-antisolvent mixture used in SDS. Presumably, differences measured in size can be attributed to the increased probability of collision at lower molecular weight. At lower molecular weight and constant polymer concentration, the number of polymer molecules in solution is considerably higher und so the collision probability during nucleation. The investigation of different molecular weights in the BT setup did only show to have a minor influence (193.3 ± 2.1 nm with 7000–17,000 g/mol vs. 181.7 ± 0.5 nm with 38,000–54,000 g/mol) as also put together by Lepeltier et al. [39]. Again, the influence of diffusion does not seem to be pronounced. In Fig. 4A–E SEM micrographs are displayed which clearly demonstrate the differences in particle size obtained using different types of PLGA.

3.2.3. *Effect of spinning speed and dropping position*

Since the spinning speed of the rotating plate could only be set indirectly via the voltage of the applied power source, the rotational speeds of the rotating plate were reproducible, but could not be set freely. Three speeds were tested with the largest possible differences. The particles produced had similar sizes (841 rpm: 140.9 ± 1.3 nm, 2051 rpm: 146.5 ± 11.2 nm and 2727 rpm: 139.2 ± 9.4 nm) with small distributions (PDI <0.05).

In contrast, Sana et al. [23] and Khan and Rathod [24] report smaller particles at higher rotational speeds (400–1200 and 500–3000 rpm). This was argued with an increased micromixing due to the increased centrifugal forces on the plate, which reduces the probability of collision and thus particle growth [25]. Furthermore, in our setup different dropping positions had no relevant changes or correlating tendencies in particle size (0 cm: 140.9 ± 1.3 nm, 1.5 cm: 126.4 ± 2.0 nm and 3 cm: 134.0 ± 2.4 nm). All PDIs indicated small size distributions (PDI <0.05). De Caprariis et al. [16] reported a decrease in particle size with increasing distance from the center of the rotating plate. Again, they claimed a more efficient micromixing with increasing distance as possible reason. Since in the mentioned publications two separate feeding jets were used and therefore micromixing had an essential influence on the size of the particles, which is conclusive considering the setup. In our case, micromixing does not affect particle production because pre-mixed, homogeneous liquids were applied to the rotating plate. In our setup, with an increased rotational speed or with increasing distance of the dropping position from the center of the spinning disc, the dripped solution should be driven faster to the rim and thus the polymers saturate with ongoing evaporation and the polymers and nuclei should increase the distance between each other due to radial forces. Thus, smaller particles would be expected due to shorter residence times limiting particle growth. However, since an increase in the rotational speed is accompanied by a faster evaporation of the solvent (see Fig. 7B) and the polymers reach solubility limit earlier leading to precipitation. Larger particles would be the result. Both effects will contribute but a different setup would be necessary to enable visualizing the effect.

3.2.4. *Effect of solvent and antisolvent type*

Using different solvents, a change in particle size was observed in SEM and DLS (Fig. 4F–H, Fig. 5). With ACN and THF larger particles were formed (approx. 230 nm) than with ACE (approx. 140 nm; Fig. 5). Huang and Zhang also reported that solutions in the BT process had an influence on particle size. They found that ACE and ACN resulted in approximately equal particle sizes, while THF led to larger particles. This phenomenon is connected also to different diffusion coefficients of the organic solvents into water [33] as this leads to faster and better micromixing [39] which is also observed in respective inverse nanoprecipitation [40]. However, as a premixed solvent-water mixture was applied in SDS, this effect probably does not explain the resulting particle sizes. Surface tension of the different solvents also has an influence on particle sizes influencing supersaturation [32]. By decreasing surface tension, the polymers to be concentrated are distributed to a higher extent thus being more distanced on the spinning disc with the same contact time. This reduces the probability of collision and particle growth is more limited. In literature average values for surface tensions of 23.122 Nm^{-1} for ACE, 27.340 Nm^{-1} for THF and 29.143 Nm^{-1} for ACN can be found [41]. Fig. 4F–H shows SEM images of PLGA nanoparticles prepared just by drying the solvent-antisolvent mixtures on silica wafers. By changing the solvent from ACE to ACN or the non-solvent from H_2O to ethanol a visual increase in size as a result of the drying process alone can be seen. Consequently, evaporation pressure will be involved in particle formation as the vapor pressure should affect the speed with which supersaturation is reached (which is fitting to the order of ACE, ACN and THF and our results).

A change in the antisolvent from water to alcohols also caused a change in size. The precipitation in methanol, ethanol and isopropanol led to particle sizes of approx. 210–220 nm (Fig. 5). This result could be attributed to the interaction between polymer and antisolvent, which is reflected by the Hansen solubility parameters: PLGA 20.20 $MPa^{1/2}$, water 47.8 $MPa^{1/2}$, ethanol 26.52 $MPa^{1/2}$, methanol 29.61 $MPa^{1/2}$ and isopropanol 23.58 $MPa^{1/2}$ [42,43]. The hydrophobic PLGA is generally insoluble in both water and alcohols. However, according to the Hansen solubility parameter, it is significantly less soluble in water than in the alcohols tested. As a consequence, the precipitation process in alcohols might be slower, thus, particle growth lasts for a longer time, whereas complete precipitation in water is completed earlier, with a lower growth rate and thus smaller particles. To support this hypothesis, further investigations should be carried out.

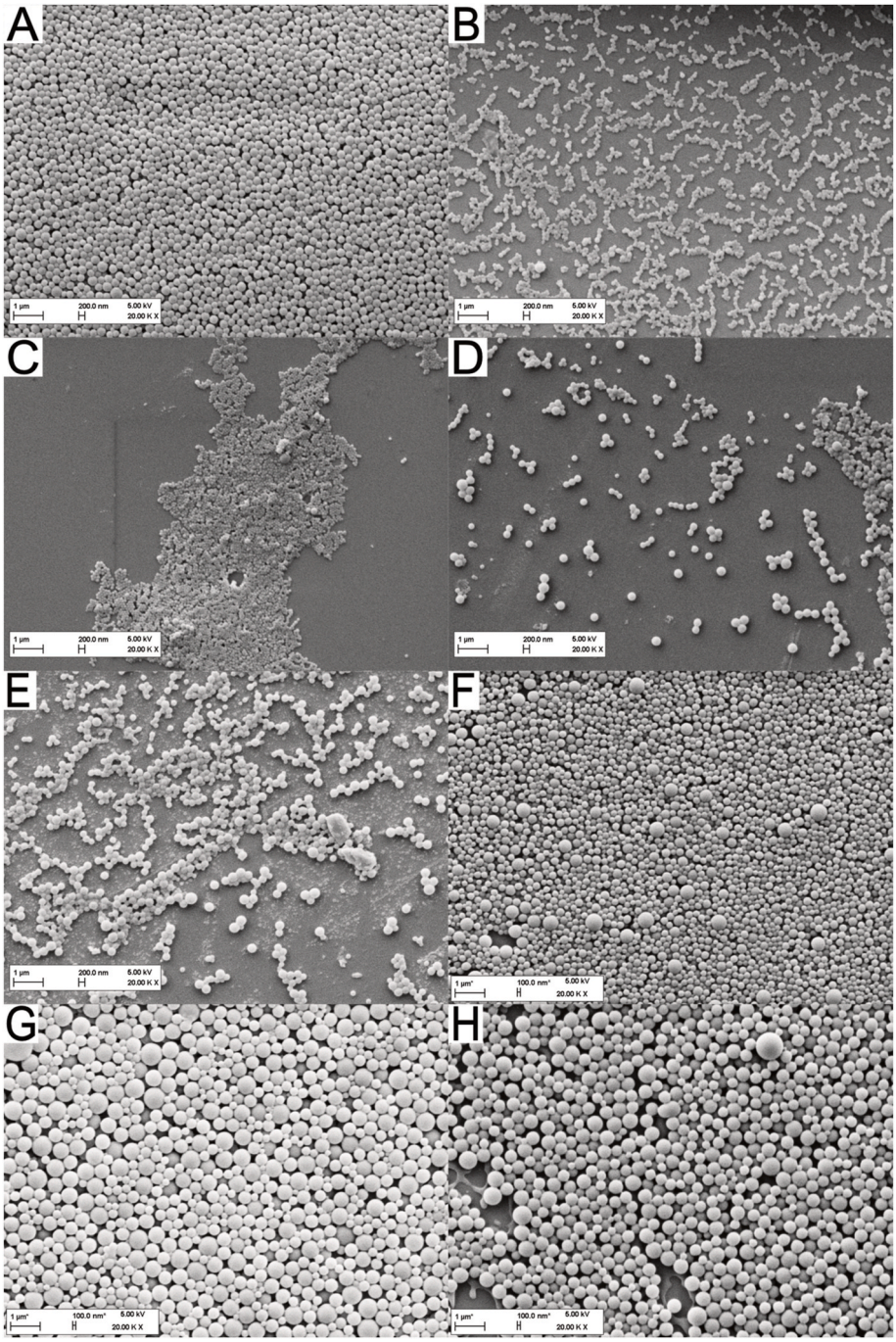

Fig. 4. SEM images of PLGA nanoparticles. A–E: Different PLGA types in ACE and H_2O precipitated by SDS. A: Resomer RG 502H (50 % LA content, 7–17,000 g/mol), 241 ± 34 nm. B: Resomer RG 503H (50 % LA content, 24–38,000 g/mol), 127 ± 21 nm. C: Resomer RG 504H (50 % LA content, 38–54,000 g/mol), 84 ± 20 nm. D: Resomer RG 653H (65 % LA content, 24–38,000 g/mol), 198 ± 38 nm. E: Resomer RG 753H (75 % LA content, 24–38,000 g/mol), 227 ± 45 nm. F–H: Resomer RG 503H precipitated in different solvent-antisolvent mixtures by drying on silica wafers. F: ACE and H_2O, 183 ± 65 nm. G: ACN and H_2O, 386 ± 115 nm. C: H: ACE and ethanol, 348 ± 86 nm. Diameters of 30 particles were measured in each image.

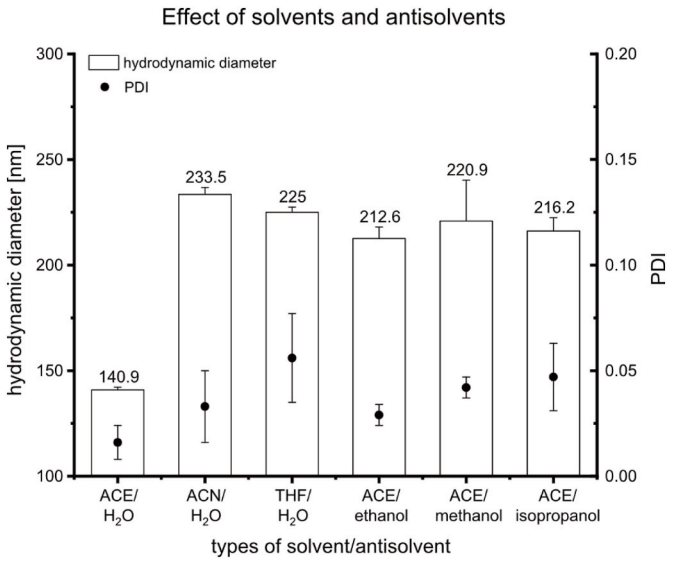

Fig. 5. Effect of solvents and antisolvents on nanoparticle sizes. Resomer RG 503H dissolved in different solvent/antisolvent variations in SDS.

3.3. Yield of SDS produced nanoparticles

The determination of the yield showed lower particle yields with higher polymer concentrations. Thus, yields of 88.8 ± 2.1 % at 2 mg/ml, 72.8 ± 4.8 % at 6 mg/ml and 40.6 ± 2.7 % at 12 mg/ml of the PLGA quantity were recovered. The polymer loss is due to the PLGA particles dried on the spinning disc (Fig. 1B). The higher the concentrations, the earlier supersaturation will be reached. Thus, more particles will be created early in the process and can dry on the disc before they reach the edge and could be collected. Up to a center distance of approximately 3 cm, no or a rather small amount of PLGA seemed to remain on the plate. Behind this distance, the resulting particle suspension flowed radially towards the edge. Most of the polymer loss seems to be in the rays. It can be assumed that the different areas on the plate are due to a change in surface tension and thus wettability of the liquid, caused by evaporation of the solvent. Furthermore, we assume that precipitation of the particles has taken place before they reach the rim, so that probably an adjustment of the plate size to reduce the loss seems possible. In the BT process, where particles usually have to be purified, this also results in a loss of yield. For example, by purification of the particles by centrifugation the yield depends on centrifugation conditions and particle size. Smaller sizes tend to produce more particle loss and accordingly behave contrary to the SDS. In addition, the quality of the particles suffers in BT due to aggregate formation and partially incomplete redispersibility after centrifugation [44].

3.4. Colloidal stability of SDS produced nanoparticles

All investigated particles did not show any visible or measurable changes in stability such as caking of agglomerated nanoparticles, a decrease of the ζ-potential and a subsequent increase in particle size and PDI due to agglomeration. For example, the maximum size deviation after 28 days stored at 4 °C for all investigated particles was between 2 and 6 nm. Accordingly, the particle size remained constant over the measured time. The size distributions showed slight fluctuations, but all PDIs remained below 0.1 (Table 1). The average maximum decrease in ζ-potential was 5.6 mV (PVA coated plates) and 7.6 mV (not coated plates). All in all, all measured ζ−potentials were below values of −30 mV (−39 ± 2 mV) and therefore showed good stability even after 28 days. Thus, comparing the data obtained using an uncoated rotating disc and a disc coated with PVA it can be concluded that the coating of the plate with a stabilizer (*e.g.*, PVA) is not necessary to maintain particles' colloidal quality, at least, for storage of 28 days. For longer storage periods further studies should be carried out. The stability of the particles produced in prototype II can also be assured (supplementary material).

Table 1
Stability of PLGA nanoparticles prepared by SDS. Maximum deviations occurring within 28 days in particle size, PDI and ζ-potential (ζ-p) from the freshly produced particles are shown when storing the particles at 4 °C. Means and standard deviations of these maximum deviations are calculated out of three independent batches (n = 3).

sample	PVA coated plates			Not coated plates		
	Size [nm]	*PDI*	*ζ-p [mV]*	*Size [nm]*	*PDI*	*ζ-p [mV]*
batch 1	6	0.0089	5.5	2	0.016	5.2
batch 2	4	0.0145	5.5	4	0.0234	8.8
Batch 3	3	0.0132	5.7	2	0.0244	8.7
mean	4	0.012	5.6	3	0.021	7.6
Standard deviation	1	0.002	0.1	1	0.004	1.7

3.5. Loading properties of CUR-loaded NPs

Particle sizes of the CUR-loaded nanoparticles (Fig. 6A and C) produced in both SDS and BT process were similar to those of unloaded particles (Fig. 2A and B). Accordingly, loading in these concentration ranges did not have an influence on particle sizes.

In SDS an increase of the polymer concentration with a constant initial load of 1 % (w/w) CUR led to an increased DL (Fig. 6B). This also resulted in a higher EE at a concentration of 6 mg/ml compared to 2 mg/ml. In contrast, at even higher concentrations of 12 mg/ml, EE was lower compared to 2 mg/ml. Since EE was calculated by multiplying the amount of drug recovered in 1 mg formulation by the yield of the formulation to obtain the total amount of drug recovered in the prepared sample, EE directly correlates to the yield. The increased DL could not compensate for the much higher particle loss (79.6 % vs. 43.5 % yield, Fig. 6B). Choi et al. [44] also reported higher DL for larger particles. Larger particles lead to larger particle volumes, which results in more drug in the particles.

In order to be able to compare loading properties in the two manufacturing processes, polymer concentrations were selected in order to obtain similar particle sizes. Fig. 6D shows that higher DL and EE could be achieved with the SDS. The DL of SDS particles is twice as high as the one of BT particles (approx. 80–90 % of the initial used CUR per mass of the polymer compared to approx. 40–45 %). Also, the EE of SDS particles (approx. 60–70 %) was pronounced higher than that of BT particles, which were several times at 10–25 %. On the one hand, this is due to the mentioned particle loss during purification for the BT particles, on which the EE depends (Chapter 3.3). On the other hand, in the BT process more CUR can be lost in the aqueous phase. The 20fold larger volume of the aqueous phase in BT (10 ml vs 0.5 ml in the SDS) containing also surfactant (2 % (w/v) PVA), enables more solubilized CUR not being available for encapsulation in the particles.

3.6. Particle production with set up for continuous production (prototype II)

The particles produced by prototype II resulted in a size of 135.5 ± 5.5 nm, a PDI of 0.017 ± 0.002 and a zeta potential of −29.2 ± 3.2 mV. Thus, the resulting particles had comparable properties to those produced with prototype I (140.9 ± 1.3 nm, PDI 0.016 ± 0.008, −28.3 ± 2.7 mV). The stability of the particles was also successfully tested (Table S1 and Table S2). At an initial test volume of 20 ml, it was difficult to collect the produced particles due to the low final volume of dispersion, so it was necessary to moisten the collection vessel additionally with water. This increased the final volume and diluted the final

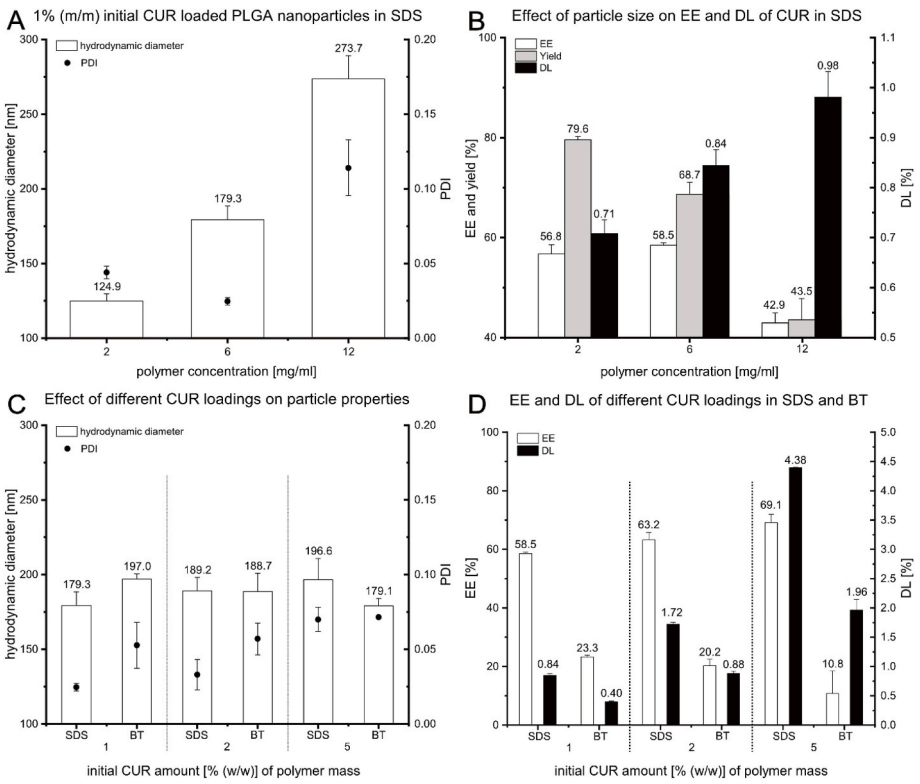

Fig. 6. Curcumin loading in SDS and BT. A: DLS results of 1 % (w/w) CUR loading with different polymer concentrations. B: EE, DL and yield of 1 % (w/w) CUR loading with different polymer concentrations. C: DLS results of different CUR loadings in SDS and BT. D: EE and DL of different CUR loadings in SDS and BT.

Table 2
Comparison of particle yield - prototype I vs. prototype II. Deviation of yields was calculated using initially 2, 6 and 12 mg/ml polymer for particle production.

Polymer Concentration	2 mg/ml	6 mg/ml	12 mg/ml
Yield Prototype I [%]	88.8	72.8	40.6
Yield Prototype II [%]	78.7	69.9	25.4
Deviation [%]	10.1	2.9	15.1
Mean [%]	9.4		
Standard deviation [%]	5.0		

dispersion. The collection of the particles without interference with the production on the spinning disc will enable the use of larger volumes (unlimited) and thus to harvest the particles continuously obtaining larger amounts of the particle dispersion. Consequently, no additional water for moisturizing would be necessary. Determinations of the yields showed an average reduction of 9.4 ± 5 % compared to prototype I (Table 2). This is probably due to the fact that the collection vessel provides more surface area for particle loss. For producing larger volumes of the dispersion, the losses should become less relevant.

3.7. Quantification of residual solvent

One of the advantages of using SDS is that the final NPs suspension is almost free of the organic solvent. HPLC analysis was used to quantify the exact amount of organic solvent present in the NPs suspension. It can be seen in Fig. 7 that after 60 min of preparation, organic solvent is almost completely removed (99.7 %) during the process. Even right after the preparation, only 4.1 % v/v of organic solvent is present in the

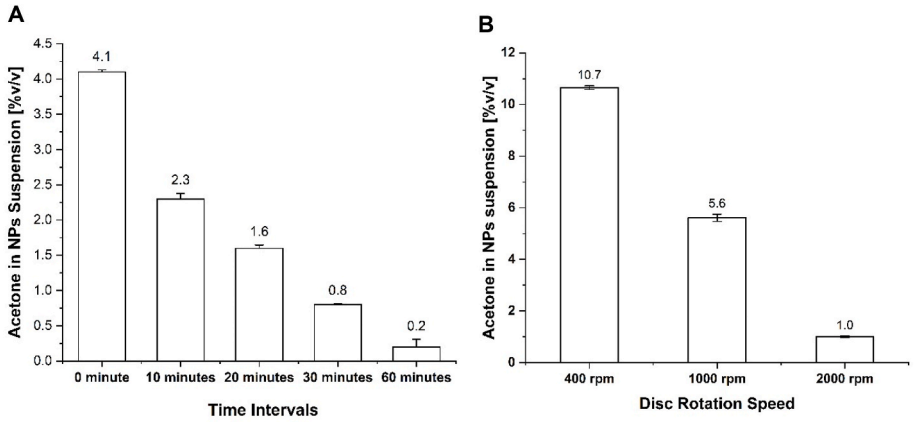

Fig. 7. Acetone removal during particle preparation with the spinning disc setup. Results of HPLC analysis for quantifying the amount of residual acetone (%v/v) at (A) different time intervals after the preparation of PLGA nanoparticles and (B) at different disc rotation speed evaluated directly after preparation (0 min). [Mean ± SD, n = 3 (represents three measurements in HPLC)].

nanoparticle's suspension, showing 95.4 % of organic solvent is removed and then followed by 97.4 %, 98.2 % and 99.1 % of removal after 10, 20 and 30 min respectively. These results underline that the SDS is able to remove almost all of the organic solvent that was used in the manufacturing of NPs.

4. Conclusion

With evaporation-triggered nanoprecipitation in SDS, a successful production of PLGA NP in the form of a highly concentrated dispersion is possible. Nanoparticle sizes can be adjustable in the range between 120 and 380 nm. The sizes depend strongly on polymer concentration and solvent-antisolvent combination as already described for nano-precipitation in BT or microfluidics. Interestingly, the hydrophobicity (LA content) and the inherent viscosity of the PLGA played a crucial role. Contrary to the current literature, no influence of the rotational speed and the dropping position on the rotating plate could be demonstrated with our set-up which is most likely an inherent limitation due to the setup. Compared to the BT method, the type of polymer had a measurable influence on particle size and a change in polymer concentration showed a more sensitive controllability of particle size and enables to tune particle sizes in a wider range (120–380 nm in SDS vs. 150–250 nm in BT). A relatively high yield of 70–90 % could be achieved for small particle sizes (<200 nm), since purification steps are not necessary, and the organic phase was already removed by evaporation during the process. Preliminary tests on the colloidal stability of the produced nanoparticles revealed that the use of stabilizers is not necessary for a sustained stability of the nanoparticles over the tested period of one month (in MilliQ water). A further strength of the setup was revealed investigating drug loading. CUR as a hydrophobic, model drug could be successfully incorporated in the NPs produced with the SDS. The EE with values of 60–70 % was three to seven times higher than for the BT approach. With increasing polymer concentration and thus also increasing particle size, up to 100 % of CUR could be encapsulated. The production of larger batches with the help of a collection vessel with an outlet drain system (prototype II) was successful and the particle size was conserved compared to prototype I. The setup potentially allows for continuous production by simple increase of the starting volume. The specific realization and the connect yield still needs to be evaluated in the future, especially considering the drying effects on the spinning disc.

CRediT authorship contribution statement

Alexandra J. Zander: Writing – original draft, Investigation. **Marie-Sophie Ehrlich:** Investigation. **Saad ur Rehman:** Writing – review & editing, Methodology, Investigation. **Marc Schneider:** Writing – review & editing, Funding acquisition, Conceptualization.

Declaration of competing interest

The authors declare that they have no known competing financial interests or personal relationships that could have appeared to influence the work reported in this paper.

Acknowledgements

Thanks to Peter Meiers and Britta Schreiber for their help in implementing the ideas for the construction of the spinning disc systems. SUR acknowledges financial support by EU- project GreenX3. This project is funded by the European Union Horizon Europe MSCA Doctoral network program under EC Grant Agreement 101120061 and by UK Research and Innovation (UKRI) under UK government's Horizon Europe funding guarantee [grant number EP/y032039].

Appendix A. Supplementary data

Supplementary data to this article can be found online at https://doi.org/10.1016/j.jddst.2025.106901.

Data availability

Data will be made available on request.

References

[1] K. Park, S. Skidmore, J. Hadar, J. Garner, H. Park, A. Otte, B.K. Soh, G. Yoon, D. Yu, Y. Yun, B.K. Lee, X. Jiang, Y. Wang, Injectable, long-acting PLGA formulations: analyzing PLGA and understanding microparticle formation, J. Contr. Release 304 (2019) 125–134, https://doi.org/10.1016/j.jconrel.2019.05.003.
[2] N. Günday Türeli, A. Torge, J. Juntke, B.C. Schwarz, N. Schneider-Daum, A. E. Türeli, C.-M. Lehr, M. Schneider, Ciprofloxacin-loaded PLGA nanoparticles against cystic fibrosis P. aeruginosa lung infections, Eur. J. Pharm. Biopharm. 117 (2017) 363–371, https://doi.org/10.1016/j.ejpb.2017.04.032.
[3] K.K. Chereddy, C.-H. Her, M. Comune, C. Moia, A. Lopes, P.E. Porporato, J. Vanacker, M.C. Lam, L. Steinstraesser, P. Sonveaux, H. Zhu, L.S. Ferreira, G. Vandermeulen, V. Préat, PLGA nanoparticles loaded with host defense peptide LL37 promote wound healing, J. Contr. Release 194 (2014) 138–147, https://doi.org/10.1016/j.jconrel.2014.08.016.
[4] D. Primavessy, N. Günday Türeli, M. Schneider, Influence of different stabilizers on the encapsulation of desmopressin acetate into PLGA nanoparticles, Eur. J. Pharm. Biopharm. 118 (2017) 48–55, https://doi.org/10.1016/j.ejpb.2016.12.003.
[5] T. Feczkó, J. Tóth, G. Dósa, J. Gyenis, Optimization of protein encapsulation in PLGA nanoparticles, Chem. Eng. Process: Process Intensif. 50 (2011) 757–765, https://doi.org/10.1016/j.cep.2011.06.008.
[6] C.B. Roces, D. Christensen, Y. Perrie, Translating the fabrication of protein-loaded poly(lactic-co-glycolic acid) nanoparticles from bench to scale-independent production using microfluidics, Drug. Delivery. Trans. Res. 10 (2020) 582–593, https://doi.org/10.1007/s13346-019-00699-y.
[7] N. Nafee, S. Taetz, M. Schneider, U.F. Schaefer, C.-M. Lehr, Chitosan-coated PLGA nanoparticles for DNA/RNA delivery: effect of the formulation parameters on complexation and transfection of antisense oligonucleotides, Nanomed. Nanotechnol. Biol. Med. 3 (2007) 173–183, https://doi.org/10.1016/j.nano.2007.03.006.
[8] R. Rietscher, C. Thum, C.M. Lehr, M. Schneider, Semi-automated nanoprecipitation-system–an option for operator independent, scalable and size adjustable nanoparticle synthesis, Pharm. Res. 32 (2015) 1859–1863, https://doi.org/10.1007/s11095-014-1612-z.
[9] J. Hiemer, A. Clausing, T. Schwarz, K. Stöwe, MicroJet reactor technology: an automated, continuous approach for nanoparticle syntheses, Chem. Eng. Technol. 42 (2019) 2018–2027, https://doi.org/10.1002/ceat.201900083.
[10] S. Schiller, A. Hanefeld, M. Schneider, C.M. Lehr, Focused ultrasound as a scalable and contact-free method to manufacture protein-loaded PLGA nanoparticles, Pharm. Res. 32 (2015) 2995–3006, https://doi.org/10.1007/s11095-015-1681-7.
[11] P.M. Valencia, O.C. Farokhzad, R. Karnik, R. Langer, Microfluidic technologies for accelerating the clinical translation of nanoparticles, Nat. Nanotechnol. 7 (2012) 623–629, https://doi.org/10.1038/nnano.2012.168.
[12] S. Ding, N. Anton, T.F. Vandamme, C.A. Serra, Microfluidic nanoprecipitation systems for preparing pure drug or polymeric drug loaded nanoparticles: an overview, Expet Opin. Drug Deliv. 13 (2016) 1447–1460, https://doi.org/10.1080/17425247.2016.1193151.
[13] K.V.K. Boodhoo, R.J. Jachuck, Process intensification: spinning disk reactor for styrene polymerisation, Appl. Therm. Eng. 20 (2000) 1127–1146, https://doi.org/10.1016/S1359-4311(99)00071-X.
[14] D. Ghiasy, M.T. Tham, K.V.K. Boodhoo, Control of a spinning disc reactor: an experimental study, Ind. Eng. Chem. Res. 52 (2013) 16832–16841, https://doi.org/10.1021/ie4020149.
[15] P. Oxley, C. Brechtelsbauer, F. Ricard, N. Lewis, C. Ramshaw, Evaluation of spinning disk reactor technology for the manufacture of pharmaceuticals, Ind. Eng. Chem. Res. 39 (2000) 2175–2182, https://doi.org/10.1021/ie990869u.
[16] B. de Caprariis, M. Di Rita, M. Stoller, N. Verdone, A. Chianese, Reaction-precipitation by a spinning disc reactor: influence of hydrodynamics on nanoparticles production, Chem. Eng. Sci. 76 (2012) 73–80, https://doi.org/10.1016/j.ces.2012.03.043.
[17] S. Mohammadi, A. Harvey, K.V.K. Boodhoo, Synthesis of TiO2 nanoparticles in a spinning disc reactor, Chem. Eng. J. 258 (2014) 171–184, https://doi.org/10.1016/j.cej.2014.07.042.
[18] K.J. Hartlieb, C.L. Raston, M. Saunders, Controlled scalable synthesis of ZnO nanoparticles, Chem. Mater. 19 (2007) 5453–5459, https://doi.org/10.1021/cm0715646.
[19] S.F. Chin, K.S. Iyer, C.L. Raston, M. Saunders, Size selective synthesis of superparamagnetic nanoparticles in thin fluids under continuous flow conditions, Adv. Funct. Mater. 18 (2008) 922–927, https://doi.org/10.1002/adfm.200701101.
[20] N. Smith, C. Raston, M. Saunders, R. Woodward, Synthesis of Magnetic Nanoparticles Using Spinning Disc Processing, 2006.

[21] J.W. Loh, J. Schneider, M. Carter, M. Saunders, L.-Y. Lim, Spinning disc processing technology: potential for large-scale manufacture of chitosan nanoparticles, J. Pharmaceut. Sci. 99 (2010) 4326–4336, https://doi.org/10.1002/jps.22145.
[22] N. Anantachoke, M. Makha, C.L. Raston, V. Reutrakul, N.C. Smith, M. Saunders, Fine tuning the production of nanosized β-Carotene particles using spinning disk processing, J. Am. Chem. Soc. 128 (2006) 13847–13853, https://doi.org/10.1021/ja063545n.
[23] S. Sana, K. Boodhoo, V. Zivkovic, Production of starch nanoparticles through solvent-antisolvent precipitation in a spinning disc reactor, in: Green Processing and Synthesis, 2019, p. 507, https://doi.org/10.1515/gps-2019-0019.
[24] W.H. Khan, V.K. Rathod, Process intensification approach for preparation of curcumin nanoparticles via solvent–nonsolvent nanoprecipitation using spinning disc reactor, Chem. Eng. Process: Process Intensif. 80 (2014) 1–10, https://doi.org/10.1016/j.cep.2014.03.011.
[25] K.V.K. Boodhoo, S.R. Al-Hengari, Micromixing characteristics in a small-scale spinning disk reactor, Chem. Eng. Technol. 35 (2012) 1229–1237, https://doi.org/10.1002/ceat.201100695.
[26] A. Aoune, C. Ramshaw, Process intensification: heat and mass transfer characteristics of liquid films on rotating discs, Int. J. Heat Mass Tran. 42 (1999) 2543–2556, https://doi.org/10.1016/S0017-9310(98)00336-6.
[27] M. Akhtar, P. Chan, N. Safriani, B. Murray, G. Clayton, Concentration of apple juice using spinning disc reactor technology, J. Food Process. Technol. 2 (2011), https://doi.org/10.4172/2157-7110.1000108.
[28] B. Almería, A. Gomez, Electrospray synthesis of monodisperse polymer particles in a broad (60nm–2μm) diameter range: guiding principles and formulation recipes, J. Colloid Interface Sci. 417 (2014) 121–130, https://doi.org/10.1016/j.jcis.2013.11.037.
[29] H. Fessi, F. Puisieux, J.P. Devissaguet, N. Ammoury, S. Benita, Nanocapsule formation by interfacial polymer deposition following solvent displacement, Int. J. Pharm. 55 (1989) R1–R4, https://doi.org/10.1016/0378-5173(89)90281-0.
[30] J.P. Rao, K.E. Geckeler, Polymer nanoparticles: preparation techniques and size-control parameters, Prog. Polym. Sci. 36 (2011) 887–913, https://doi.org/10.1016/j.progpolymsci.2011.01.001.
[31] I.J. Joye, D.J. McClements, Production of nanoparticles by anti-solvent precipitation for use in food systems, Trends Food Sci. Technol. 34 (2013) 109–123, https://doi.org/10.1016/j.tifs.2013.10.002.
[32] S.M. D'Addio, R.K. Prud'homme, Controlling drug nanoparticle formation by rapid precipitation, Adv. Drug Deliv. Rev. 63 (2011) 417–426, https://doi.org/10.1016/j.addr.2011.04.005.
[33] W. Huang, C. Zhang, Tuning the size of poly(lactic-co-glycolic acid) (PLGA) nanoparticles fabricated by nanoprecipitation, Biotechnol. J. 13 (2018) 1700203, https://doi.org/10.1002/biot.201700203.
[34] R.H. Müller, R. Schuhmann, Teilchengrößenmessung Der Laborpraxis, Wissenschaftliche Verlagsgesellschaft mbH Stuttgart, 1996.
[35] U. Bilati, E. Allémann, E. Doelker, Development of a nanoprecipitation method intended for the entrapment of hydrophilic drugs into nanoparticles, Eur. J. Pharmaceut. Sci. 24 (2005) 67–75, https://doi.org/10.1016/j.ejps.2004.09.011.
[36] A. Budhian, S.J. Siegel, K.I. Winey, Haloperidol-loaded PLGA nanoparticles: systematic study of particle size and drug content, Int. J. Pharm. 336 (2007) 367–375, https://doi.org/10.1016/j.ijpharm.2006.11.061.
[37] X. Yan, J. Bernard, F. Ganachaud, Nanoprecipitation as a simple and straightforward process to create complex polymeric colloidal morphologies, Adv. Colloid Interface Sci. 294 (2021) 102474, https://doi.org/10.1016/j.cis.2021.102474.
[38] C.I.C. Crucho, M.T. Barros, Polymeric nanoparticles: a study on the preparation variables and characterization methods, Mater. Sci. Eng. C 80 (2017) 771–784, https://doi.org/10.1016/j.msec.2017.06.004.
[39] E. Lepeltier, C. Bourgaux, P. Couvreur, Nanoprecipitation and the "ouzo effect": application to drug delivery devices, Adv. Drug Deliv. Rev. 71 (2014) 86–97, https://doi.org/10.1016/j.addr.2013.12.009.
[40] S.A. Khan, M. Schneider, Stabilization of gelatin nanoparticles without crosslinking, Macromol. Biosci. 14 (2014) 1627–1638, https://doi.org/10.1002/mabi.201400214.
[41] Dortmund_Data_Bank, DDBST GmbH. www.ddbst.com, 2020.
[42] C.G. Madsen, A. Skov, S. Baldursdottir, T. Rades, L. Jorgensen, N.J. Medlicott, Simple measurements for prediction of drug release from polymer matrices – solubility parameters and intrinsic viscosity, Eur. J. Pharm. Biopharm. 92 (2015) 1–7, https://doi.org/10.1016/j.ejpb.2015.02.001.
[43] C.M. Hansen, Hansen Solubility Parameter: a User's Handbook, second ed. ed., CRC Press, Boca Raton, 2007.
[44] J.S. Choi, J. Cao, M. Naeem, J. Noh, N. Hasan, H.K. Choi, J.W. Yoo, Size-controlled biodegradable nanoparticles: preparation and size-dependent cellular uptake and tumor cell growth inhibition, Colloids Surf. B Biointerfaces 122 (2014) 545–551, https://doi.org/10.1016/j.colsurfb.2014.07.030.